

Time Delay in Black Hole Gravitational Lensing as a Distance Estimator

V. Bozza^{a,b,c}, L. Mancini^{b,c,d}

^a *Centro studi e ricerche “Enrico Fermi”, Rome, Italy.*

^b *Dipartimento di Fisica “E. R. Caianiello”, Università di Salerno, 84081 Baronissi, Italy.*

^c *Istituto Nazionale di Fisica Nucleare, Sezione di Napoli, Italy.*

^d *Institut für Theoretische Physik der Universität Zürich, CH-8057 Zürich, Switzerland.*

(Dated: September 11, 2018)

We calculate the time delay between different relativistic images formed by black hole gravitational lensing in the strong field limit. For spherically symmetric black holes, it turns out that the time delay between the first two images is proportional to the minimum impact angle. Their ratio gives a very interesting and precise measure of the distance of the black hole. Moreover, using also the separation between the images and their luminosity ratio, it is possible to extract the mass of the black hole. The time delay for the black hole at the center of our Galaxy is just few minutes, but for supermassive black holes with $M = 10^8 \div 10^9 M_\odot$ in the neighbourhood of the Local Group the time delay amounts to few days, thus being measurable with a good accuracy.

PACS numbers: 95.30.Sf, 04.70.Bw, 98.62.Sb

Keywords: Relativity and gravitation; Classical black holes; Gravitational lensing

I. INTRODUCTION

Gravitational lensing is a useful tool to investigate a lot of aspects of the nature of the universe. It was the first prove of the validity of the theory of general relativity (GR) [1], and today its effects on extragalactic scales (lensing of quasars, arcs in galaxy clusters, etc.) and on galactic scales (microlensing) are ordinarily observed and studied by the scientific community in the weak field approximation [2].

In the last years, a new form of gravitational lensing has been proposed as a method to investigate the gravitational field generated by collapsed objects. This approach considers light rays of background sources passing very close to the event horizons of black holes without entering inside. The study of this extreme case is of remarkable interest: on one hand it represents an independent test of GR in strong gravitational fields; on the other hand, intrinsic features of the lens (rotation, electric charge, etc.) could become accessible to the observations, opening a new possibility to constrain black hole models.

In Schwarzschild framework, a light ray with small impact parameter can wind several times around a black hole without being definitively caught inside. In this way, a set of infinite relativistic images can be generated on each side of the black hole [3, 4]. Several approaches have been proposed to study gravitational lensing in the strong field limit [4, 5, 6, 7, 8, 9, 10], while Falcke, Melia & Agol, in a different perspective, studied the accretion flow as a source [11]. In Ref. [12] analytical formulae for the position and the magnification of the images were obtained, defining a *strong field limit* for the deflection angle. These formulae were applied to a Reissner-Nordstrom black hole in Ref. [13], and were also used to calculate relativistic effects on microlensing events [14]. A full generalization of the strong field limit for any spherically symmetric spacetime was drawn in Ref. [15] and applied to several black hole met-

rics, allowing a non-degenerate discrimination among different collapsed objects. In work [16], the method was used to examine the characteristics of a Gibbons-Maeda-Garfinkle-Horowitz-Strominger charged black hole of heterotic string theory. In work [17] the case of a Kerr black hole and the relevance of its spin in strong field lensing approximation was discussed for light rays travelling on quasi-equatorial trajectories. Waiting for an analytical treatment including non-equatorial trajectories, the general case is explored numerically in [18].

When multiple images are formed, the light-travel-time along light paths corresponding to different images is generally not the same. So, if the source is characterized by luminosity variations, these variations would show up in the images with a relative temporal phase depending on the geometry of the lens [19]. These time delays are usually measured in gravitational lensing observations on cosmological scales. The striking importance of time delay lies in the fact that it is the only dimensional observable. Therefore its measurement is useful to determine at first the length scale for a gravitational lensing system and its mass. Measuring the time delays in cosmological contexts, it is possible to determine the cosmological distance scale and hence the Hubble parameter [19, 20, 21]. This fact has drawn a great attention by the scientific community towards this kind of measurements.

In the present paper, we estimate the time delay between images generated by strong field lensing of black holes. We show that time delays between relativistic images are indeed measurable in most supermassive black holes suitable for gravitational lensing studies. Moreover, it turns out that in a first approximation the time delay between consecutive relativistic images is proportional to the minimum impact angle. The ratio between these two observables is nothing but the distance of the lens, that can be estimated in a very precise way and without bias. Combining all information, it is also possible to get an independent mass estimate, to be compared with estimates

obtained by other methods.

This paper is structured as follows. In Sect. 2, we recall the main results of the strong field limit method. In Sect. 3 we derive a general expression for the time delay, specifying it to the spherically symmetric case. In Sect 4, we estimate the expected time delays for several interesting supermassive extragalactic black holes discussing the whole information that can be extracted from a time delay measurement. Finally, in Sect. 6, we draw the conclusions. An appendix contains the computation of the time delay for the Kerr metric, as an example of a non-spherically symmetric metric.

II. THE STRONG FIELD LIMIT APPROACH

The technique we use in the derivation of the time delay between different images resembles the main calculation of the deflection angle in the strong field limit approach. We shall briefly recall the main steps of that derivation referring the reader to Refs. [15, 17] for all the details.

Consider a generic black hole metric projected on the equatorial plane

$$ds^2 = A(x)dt^2 - B(x)dx^2 - C(x)d\phi^2 + D(x)dt d\phi \quad (1)$$

where $D(x)$ can be consistently set to zero in a spherically symmetric black hole.

The metric does not depend on time and the azimuthal angle ϕ , so that, for a photon moving in this background, \dot{t} and $\dot{\phi}$ can be expressed in terms of two integrals of motion, namely energy and angular momentum. By a suitable choice of the affine parameter, we set the first to 1 and the second to the impact parameter u of the incoming photon. We have

$$\dot{t} = \frac{4C - 2uD}{4AC + D^2} \quad (2)$$

$$\dot{\phi} = \frac{4Au + 2D}{4AC + D^2}. \quad (3)$$

The impact parameter u , is related to the closest approach distance x_0 by

$$u = \frac{-D_0 + \sqrt{4A_0C_0 + D_0^2}}{2A_0}, \quad (4)$$

where all functions with the subscript 0 are evaluated for $x = x_0$.

By the on-shell condition for the photon, we also derive

$$\dot{x} = \pm \frac{2}{\sqrt{B}} \sqrt{\frac{C - uD - u^2A}{4AC + D^2}}. \quad (5)$$

Dividing Eq. (3) by Eq. (5), we get

$$\frac{d\phi}{dx} = P_1(x, x_0)P_2(x, x_0) \quad (6)$$

$$P_1(x, x_0) = \frac{\sqrt{B}(2A_0Au + A_0D)}{\sqrt{CA_0}\sqrt{4AC + D^2}} \quad (7)$$

$$P_2(x, x_0) = \frac{1}{\sqrt{A_0 - A\frac{C_0}{C} + \frac{u}{C}(AD_0 - A_0D)}}. \quad (8)$$

Integrating this expression from x_0 to infinity we find half the deflection angle as a function of the closest approach. Given the symmetry between approach and departure, we can write the whole deflection angle as

$$\alpha(x_0) = \phi_f(x_0) - \pi \quad (9)$$

$$\phi_f(x_0) = 2 \int_{x_0}^{\infty} \frac{d\phi}{dx} dx. \quad (10)$$

To solve this integral, we define the variables

$$y = A(x) \quad (11)$$

$$z = \frac{y - y_0}{1 - y_0} \quad (12)$$

where $y_0 \equiv A_0$. The integral (10) in the deflection angle becomes

$$\phi_f(x_0) = \int_0^1 R(z, x_0) f(z, x_0) dz \quad (13)$$

$$R(z, x_0) = 2 \frac{1 - y_0}{A'(x)} P_1(x, x_0) \quad (14)$$

$$f(z, x_0) = P_2(x, x_0) \quad (15)$$

where $x = A^{-1}[(1 - y_0)z + y_0]$.

The function $R(z, x_0)$ is regular for all values of z and x_0 , while $f(z, x_0)$ diverges for $z \rightarrow 0$. We then expand the argument of the square root in $f(z, x_0)$ to the second order in z , defining

$$f(z, x_0) \sim f_0(z, x_0) = \frac{1}{\sqrt{\alpha z + \beta z^2}}. \quad (16)$$

The Eq. $\alpha = 0$ defines the radius of the photon sphere x_m , which is the minimum approach distance for photons not falling into the black hole.

The result of the integral (13) gives the strong field limit expansion of the deflection angle [15]

$$\alpha(u) = -\bar{a} \log\left(\frac{u}{u_m} - 1\right) + \bar{b} + O(u - u_m), \quad (17)$$

where the coefficients of the expansion are

$$u_m = \frac{-D_m + \sqrt{4A_mC_m + D_m^2}}{2A_m} \quad (18)$$

$$\bar{a} = \frac{R(0, x_m)}{2\sqrt{\beta_m}} \quad (19)$$

$$\bar{b} = -\pi + b_D + b_R + \bar{a} \log \frac{cx_m^2}{u_m} \quad (20)$$

and

$$b_D = 2\bar{a} \log \frac{2(1-y_m)}{A'_m x_m} \quad (21)$$

$$b_R = \int_0^1 [R(z, x_m) f(z, x_m) - R(0, x_m) f_0(z, x_m)] dz, \quad (22)$$

while c is defined by the expansion

$$u - u_m = c(x_0 - x_m)^2. \quad (23)$$

All the functions with the subscript m are evaluated at $x_0 = x_m$.

With the formula (17) for the deflection angle, it is straightforward to calculate the positions and the magnifications of all relativistic images. Two infinite patterns of relativistic images appear on each side of the lens, very close to the minimum impact angle $\theta_m = u_m/D_{OL}$ (D_{OL} is the distance of the lens from the observer). These images are highly demagnified unless the source is very close to a caustic point. For spherically symmetric black holes, all caustic points are exactly aligned with the lens, so that a source aligned with the optical axis (the line joining observer and lens) would enhance the magnification of all images simultaneously.

In spinning black holes, the caustics drift away from the optical axis, so that one source cannot be simultaneously close to different caustics. In this case only one image at a time can be enhanced while all others stay very faint [17]. Nevertheless, in this case, additional images, appearing when the source is inside a caustic, may play an important role in the phenomenology, yet to be understood.

For later reference, we write here the formula for the position of the relativistic images

$$\theta_n^\pm = \pm \theta_m \left(1 + e^{\frac{\bar{b} - 2n\pi \pm \gamma}{\bar{a}}} \right). \quad (24)$$

Here γ is the angular separation between the source and the optical axis, as seen from the lens. n is the number of loops done by the photon around the black hole. For each n , we have an image on each side of the lens, according to the chosen sign.

III. TIME DELAY IN THE STRONG FIELD LIMIT

In this section we derive the time delay between different relativistic images, following an approach similar to the one reported in the previous subsection for the deflection angle, but with some tricky subtraction strategies to treat the integrals.

For an observer at infinity, the time taken from the photon to travel from the source to the observer is simply

$$T = \int_{t_0}^{t_f} dt. \quad (25)$$

Changing the integration variable from t to x , we split the integral into approach and leaving phases

$$T = \int_{D_{LS}}^{x_0} \frac{dt}{dx} dx + \int_{x_0}^{D_{OL}} \frac{dt}{dx} dx. \quad (26)$$

Here D_{LS} is the distance between the source and the lens, while D_{OL} is the distance between the lens and the observer.

Extending the integration limits to infinity, we can unify the two integrals into one, exploiting the symmetry between approach and departure. This can be done at the price of subtracting two terms

$$T = 2 \int_{x_0}^{\infty} \left| \frac{dt}{dx} \right| dx - \int_{D_{OL}}^{\infty} \left| \frac{dt}{dx} \right| dx - \int_{D_{LS}}^{\infty} \left| \frac{dt}{dx} \right| dx. \quad (27)$$

If we consider two photons, travelling on different trajectories, the time delay between them is

$$\begin{aligned} T_1 - T_2 &= 2 \int_{x_{0,1}}^{\infty} \left| \frac{dt}{dx}(x, x_{0,1}) \right| dx - 2 \int_{x_{0,2}}^{\infty} \left| \frac{dt}{dx}(x, x_{0,2}) \right| dx \\ &\quad - \int_{D_{OL}}^{\infty} \left| \frac{dt}{dx}(x, x_{0,1}) \right| dx + \int_{D_{OL}}^{\infty} \left| \frac{dt}{dx}(x, x_{0,2}) \right| dx \\ &\quad - \int_{D_{LS}}^{\infty} \left| \frac{dt}{dx}(x, x_{0,1}) \right| dx + \int_{D_{LS}}^{\infty} \left| \frac{dt}{dx}(x, x_{0,2}) \right| dx. \end{aligned} \quad (28)$$

Supposing that observer and source are very far from the black hole, dt/dx is effectively 1 in the last four integrals which thus exactly cancel each other. We are thus left with the first two integrals.

Dividing Eq. (2) by Eq. (5), we obtain

$$\frac{dt}{dx} = \tilde{P}_1(x, x_0) P_2(x, x_0) \quad (29)$$

$$\tilde{P}_1(x, x_0) = \frac{\sqrt{BA_0}(2C - uD)}{\sqrt{C}\sqrt{4AC + D^2}} \quad (30)$$

and P_2 defined by Eq. (8). Of course, dt/dx tends to one for large x and the two integrals in (28) are separately divergent, while their difference is finite. In fact, the time delay is the result of the different paths followed by the photons while they wind around the black hole. When the two photons are far away from the black hole, $dt/dx \rightarrow 1$ and the two integrals compensate each other. Separating the two regimes, we can write individually convergent integrals. To achieve this, we subtract and add the function $\tilde{P}_1(x, x_{0,i})/\sqrt{A_{0,i}}$ to each integrand.

Supposing $x_{0,1} < x_{0,2}$, we can write

$$T_1 - T_2 = \tilde{T}(x_{0,1}) - \tilde{T}(x_{0,2}) + 2 \int_{x_{0,1}}^{x_{0,2}} \frac{\tilde{P}_1(x, x_{0,1})}{\sqrt{A_{0,1}}} dx$$

$$+ 2 \int_{x_{0,2}}^{\infty} \left[\frac{\tilde{P}_1(x, x_{0,1})}{\sqrt{A_{0,1}}} - \frac{\tilde{P}_1(x, x_{0,2})}{\sqrt{A_{0,2}}} \right] dx \quad (31)$$

with

$$\tilde{T}(x_0) = \int_0^1 \tilde{R}(z, x_0) f(z, x_0) dz \quad (32)$$

$$\tilde{R}(z, x_0) = 2 \frac{1 - y_0}{A'(x)} \tilde{P}_1(x, x_0) \left(1 - \frac{1}{\sqrt{A_0} f(z, x_0)} \right) \quad (33)$$

and $f(x, x_0)$ defined by Eq. (15). Substituting all the expressions back into (31), we can check that it is equivalent to (28), but now it is written as a sum of separately convergent integrals.

In practice, the integral $\tilde{T}(x_0)$ represents the time spent by the light ray to wind around the black hole. In order to cutoff the integrands at large x 's, in the definition of $R(z, x_0)$ we have subtracted a term which is negligible when the photon is close to the black hole but cancels the integrand when the photon is far from the black hole. The residual terms of this subtraction are stored in the last two integrals in (31) and are generally subleading with respect to $\Delta\tilde{T}$, as we shall see later.

The integral (32) can be solved following the same technique of the integral (13) in the previous subsection, just replacing R by \tilde{R} . The result is

$$\tilde{T}(u) = -\tilde{a} \log \left(\frac{u}{u_m} - 1 \right) + \tilde{b} + O(u - u_m) \quad (34)$$

where u_m is defined by Eq. (18) and

$$\tilde{a} = \frac{\tilde{R}(0, x_m)}{2\sqrt{\beta_m}} \quad (35)$$

$$\tilde{b} = -\pi + \tilde{b}_D + \tilde{b}_R + \tilde{a} \log \frac{cx_m^2}{u_m} \quad (36)$$

with

$$\tilde{b}_D = 2\tilde{a} \log \frac{2(1 - y_m)}{A'_m x_m} \quad (37)$$

$$\tilde{b}_R = \int_0^1 \left[\tilde{R}(z, x_m) f(z, x_m) - \tilde{R}(0, x_m) f_0(z, x_m) \right] dz. \quad (38)$$

For spherically symmetric black holes, the expression for the time delay can be advantageously simplified. Notice that, for spherically symmetric spacetimes, $D = 0$ and

$$\tilde{P}_1(x, x_0)|_{D=0} = \sqrt{\frac{BA_0}{A}}. \quad (39)$$

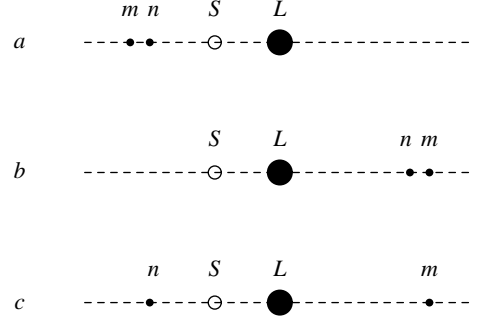


FIG. 1: This figure illustrates which images are considered in the different time delay calculations in the text. L represents the lens, S is the source. On each side of the lens an infinite series of images is formed. In case a , we consider two images on the same side of the source. Their time delay is given by $\Delta T_{n,m}^s$ with the upper sign. In case b , we consider two images appearing on the same side but opposite to the source. Their time delay is given by $\Delta T_{n,m}^s$ with the lower sign. Finally, in case c , we consider two images appearing on opposite sides. Their time delay is given by $\Delta T_{n,m}^o$.

Then the last integral in (31) identically vanishes. When $D \neq 0$, the dependence on x_0 remains through the impact parameter u which is present in Eq. (30). The second integral in (31) can be approximated substituting the integrand with $\sqrt{B_m/A_m}$ since it is practically constant throughout the (very small) integration interval. Finally, combining (34) with (17) we get a very simple expression for the first term in (31).

In writing the final formulae, we distinguish the case when the two images are on the same side of the lens from the case when the two images are on opposite sides of the lens. In the first case, we have

$$\Delta T_{n,m}^s = 2\pi(n - m) \frac{\tilde{a}}{a}$$

$$+ 2\sqrt{\frac{B_m}{A_m}} \sqrt{\frac{u_m}{c}} e^{\frac{\tilde{b}}{2\tilde{a}}} \left(e^{-\frac{2m\pi \mp \gamma}{2\tilde{a}}} - e^{-\frac{2n\pi \mp \gamma}{2\tilde{a}}} \right), \quad (40)$$

where the upper sign before γ applies if both images are on the same side of the source (Fig. 1a) and the lower sign if both images are on the other side (Fig. 1b).

If the images are on opposite sides of the lens (Fig. 1c), then

$$\Delta T_{n,m}^o = [2\pi(n - m) - 2\gamma] \frac{\tilde{a}}{a}$$

$$+ 2\sqrt{\frac{B_m}{A_m}} \sqrt{\frac{u_m}{c}} e^{\frac{\tilde{b}}{2\tilde{a}}} \left(e^{-\frac{2m\pi - \gamma}{2\tilde{a}}} - e^{-\frac{2n\pi + \gamma}{2\tilde{a}}} \right), \quad (41)$$

where the image winding n times is on the same side of the source and the other is on the opposite side.

Notice that the geometry mostly favoured for the observation of relativistic images is that with the source almost aligned with the lens, so that $\gamma \sim D_{OL}^{-1} \ll 2\pi$. Therefore

$$\Delta T_{n,n}^o \ll T_{n,m \neq n}^s \simeq T_{n,m \neq n}^o \quad (42)$$

i.e. if we evaluate the time delay between images with the same winding number on opposite sides, we generally find a value which is much smaller than the time delay between images with different winding number.

Moreover, for physically reasonable values of the coefficients \bar{a} , \bar{b} , which are all of order one, the second term at the right hand side of Eq. (41) is much smaller than the first. For example, in the Schwarzschild black hole, the time delay between the first and the second relativistic images is (in Schwarzschild units)

$$\Delta T_{2,1} = 16.57 \quad (43)$$

where the second term contributes only for 1.4% to the total time delay.

For spherically symmetric metrics, we also have the very important relation

$$\frac{\tilde{a}}{\bar{a}} = u_m. \quad (44)$$

Namely, the dominant term in the time delay is not a new independent combination of the black hole metric function and gives no further hint for the classification of the black hole. On the contrary, the subdominant term is an independent combination and could be used in principle to constrain the black hole model. However, the subdominant term would be typically hidden below the observational precision and it becomes reasonable to approximate the time delay by its dominant contribution. In this way, a very interesting surprise arises. In fact, suppose we are able to measure the time delay between the first two images. Once we restore physical units, the ratio between this time delay and the minimum impact angle is

$$\frac{\Delta T_{2,1}}{\theta_m} = 2\pi \frac{D_{OL}}{c_0}, \quad (45)$$

where c_0 is the speed of light. In principle, by this formula, we can get a very accurate estimate for the distance of the black hole and hence of the whole hosting galaxy. The feasibility of such an estimate, will be discussed in the next section.

In Appendix A, we treat the Kerr metric as an example of non-spherically symmetric black hole. In that case, most of the simplifications we have done, do not apply.

IV. TIME DELAY IN SUPERMASSIVE BLACK HOLE LENSING

In order to achieve a complete reconstruction of the characteristics of the black hole by strong field gravitational lensing, we must distinguish at least the outermost

Local Group Galaxy	Mass (M_\odot)	Distance (Mpc)	Schwarzschild $\Delta T_{2,1}$
Milky Way	2.8×10^6	0.0085	0.1 h
NGC0221 (M32)	3.4×10^6	0.7	0.2 h
NGC0224 (M31)	3.0×10^7	0.7	1.4 h

TABLE I: Estimates for the time delay for the supermassive black hole located at the centers of three galaxies in the case of Schwarzschild spacetime geometry. The masses and the distances are taken from Richstone et al. [23].

relativistic image from the others. Yet, as noted in [15], in order to achieve this, we need an optical resolution one or two orders of magnitude better than that reachable by short-term VLBI projects [22]. Therefore, relativistic images will possibly become a target for next generation projects. With this in mind, we can proceed to give estimates for time delays between the first and the second relativistic images in realistic situations.

We treat only black holes with spherical symmetry, because only in this case we have the formation at first of more than one observable image. In fact, as noted in [17], the phenomenology of spinning black holes is quite different. In particular, if the source is not inside a caustic, only one image should become visible, while all the others stay very faint. On the contrary, if the source is inside a caustic, two additional non-equatorial images should appear. But an analytical treatment for these additional images is not available at present.

Of course, we implicitly assume that the source must have temporal variations, otherwise there is no time delay to measure. Thus, an essential condition is that the source must be somehow variable. However, this is not a so restrictive requirement, since variable stars are generally abundant in all galaxies.

In Table I, we present the values of the time delay for the black hole located at the center of the Milky Way and in other two galaxies of the Local Group. The results are obtained using the Schwarzschild metric. It is clear that we have a little chance to observe such short time delays for reasonable times of exposure.

In order to have higher time delays, we need black holes with larger Schwarzschild radii, i.e. more massive black holes. At the same time we require that the magnification of the images must remain of the same order. Since we know that the magnification is proportional to M_{Lens}/D_{OL} , our request can be fulfilled if we consider lenses with a mass of two or three orders of magnitude larger than the black hole in the center of our galaxy, and located not farther than three orders of magnitude its distance. In this case, the measurement of the time delay becomes more favorable as shown in Table II, where we report our estimates for the time delay due to supermassive black holes located at the centers of not too far galaxies, according to spacetime geometry.

The time delays range from few hours to several days. It must be kept in mind that a very deep exposure is

Galaxy	Mass (M_{\odot})	Distance (Mpc)	Schwarzschild $\Delta T_{2,1}$
NGC4486 (M87)	3.3×10^9	15.3	149.3 h
NGC3115	2.0×10^9	8.4	90.5 h
NGC4374 (M84)	1.4×10^9	15.3	63.3 h
NGC4594	1.0×10^9	9.2	45.2 h
NGC4486B (M104)	5.7×10^8	15.3	25.8 h
NGC4261	4.5×10^8	27.4	20.4 h
NGC7052	3.3×10^8	58.7	14.9 h
NGC4342 (IC3256)	3.0×10^8	15.3	13.6 h
NGC3377	1.8×10^8	9.9	8.1 h

TABLE II: Estimates for the time delay for supermassive black holes located at the center of several nearby galaxies in the case of Schwarzschild spacetime geometry. The masses and the distances of the central black holes are taken from Richstone et al. [23].

needed to detect the very faint relativistic images. The precise time will depend on the characteristics of the future interferometers which will catch the relativistic images and on the power of the source. However, we can imagine that an exposure of 10 hours can be still taken as a reasonable reference value for a deep imaging of a supermassive black hole. Then, with a high enough sampling and a suitable periodicity for the variable source, we can imagine to determine the time delay with an accuracy of few hours. So, most of the black holes in Tab. II would yield measurable time delays.

Now consider the supermassive black hole in M87 and suppose we manage to reach an accuracy of 5% in a time delay measure. The resolution needed to resolve the first two images is $0.01 \mu\text{arcsecs}$, while the minimum angle is $\theta_m = 11 \mu\text{arcsecs}$. From formula (45), we can get the distance to M87 with an accuracy of 5% (the error in the angle measurement is negligible). This is already better than standard estimates by classical distance indicators [24], whose accuracy ranges from 10% to 25%.

So, gravitational lensing in the strong field limit may become a potentially competitive distance estimator in a not so far future. This is a consequence of the fact that the time delay is a dimensional variable and thus immediately leads to the measure of a scale. In the strong field frame, it is proportional to the mass of the black hole through the minimum impact parameter. However, it happens that we can also measure the minimum impact angle $\theta_m = u_m/D_{OL}$ directly, so that their ratio leaves us with the distance to the lens. A time measurement can be done with a high accuracy and has the advantage of being completely immune from any unwanted bias or systematics, unlike the classical estimates relying on luminosity measurements and typically highly model-dependent assumptions.

A measurement as simple as this cannot be realized in weak field gravitational lensing, because it requires an accurate modeling of the gravitational potential. More-

over, the length scale it measures is in general a more involved combination of all geometrical distances (D_{OL} , D_{LS} , D_{OS}).

Another interesting possibility of strong field gravitational lensing is the possibility of getting a mass estimate. By the characteristics of the first two relativistic images, we can get the coefficients \bar{a} and \bar{b} , according to the procedure described in [15]. They are generally sufficient to identify the class of the specific black hole. Afterwards, we can guess the theoretical u_m in Schwarzschild radii for the specific black hole model. Combining with the the observed θ_m and with the D_{OL} obtained by time delay, we get the Schwarzschild radius and hence the mass of the black hole. So, in principle, the time delay measurement would make the strong field gravitational lensing completely autonomous from external inputs coming from other methods.

One final consideration about the subdominant term neglected in (45): if we simply identify the time delay with its dominant contribution, we overestimate it by 1 or 2%. However, once we have identified the black hole class by the coefficients \bar{a} and \bar{b} , we can easily evaluate the expected contribution of the subdominant term on the specific black hole model and subtract it from the observed time delay. We are then left with the pure dominant term and no more systematic errors (however small) are present.

V. CONCLUSIONS

Gravitational lensing in the strong field limit may represent a key tool for the investigation of supermassive black holes. In principle, a complete characterization of the parameters of a black hole can be achieved by the study of the images formed by gravitational lensing of a background source. Technically, this study requires resolutions one or two orders of magnitudes better than actual VLBI projects, so that it stands as a possible observational target for the next future.

In this work we have pointed out that photons contributing to different strong field images take different times to reach the observer. This time delay is of order of few seconds for the black hole at the center of our Galaxy, but amounts to several days for more massive black holes at the centers of nearby galaxies.

If the background source is characterized by an intrinsic variability, it would then be possible to measure the time delay between different strong field images, with the important advantage of gaining a dimensional measurement for the scale of the system. This measurement can be immediately used to get an accurate distance determination for the observed black hole, not affected by any kind of bias or model-dependent assumption. Identifying the black hole class by the use of the other strong field limit observables, we can also derive the mass of the black hole in a completely independent way. This result encourages our belief that gravitational lensing in the

strong field limit stands as an interesting (maybe powerful) method for the classification of black holes and the determination of their characteristics. Moreover, a new independent distance determination method is always welcome in cosmological contexts.

Acknowledgments

The authors are grateful to Gaetano Scarpetta for helpful comments on the manuscript. V.B. wishes to thank the theoretical division of CERN and the Institute of Theoretical Physics of Zürich University for their hospitality.

APPENDIX A: TIME DELAY IN KERR BLACK HOLES

If the black hole is not spherically symmetric, the simplifications described at the end of Sect. III do not apply. In particular, the third integral in (31) does not identically vanish. In this appendix we work out the time delay in a Kerr black hole as an example of non-spherically symmetric black metric.

The Kerr metric projected on the equatorial plane reads

$$A(x) = 1 - \frac{1}{x} \quad (\text{A1})$$

$$B(x) = \frac{1}{1 - \frac{1}{x} + \frac{a^2}{x^2}} \quad (\text{A2})$$

$$C(x) = x^2 + a^2 + \frac{a^2}{x} \quad (\text{A3})$$

$$D(x) = 2\frac{a}{x}, \quad (\text{A4})$$

where a is the specific angular momentum of the black hole.

We start directly from Eq. (31), but we can still express the dominant term $\Delta\tilde{T}$ in a simpler form. Consider first the case of two images on the same side of the black hole. Then everything works in the same way as for spherically symmetric black holes and we get

$$\Delta\tilde{T}_{n,m}^s = 2\pi(n-m)\frac{\tilde{a}}{a}. \quad (\text{A5})$$

Of course, the values of \tilde{a} and \bar{a} depend on the sign of the spin a , i.e. they are different for photons winding in the same sense of the black hole (direct photons) and for photons winding in the opposite sense (retrograde photons).

If we wish to evaluate the time delay between two relativistic images appearing on opposite sides of the black

hole, then we have to take care of the fact that one image will be direct and the other will be retrograde. We then

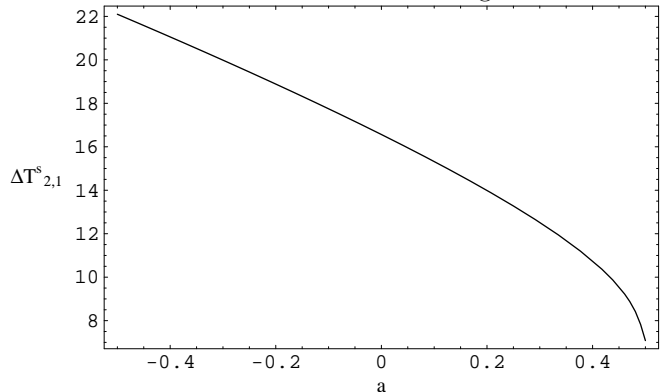


FIG. 2: Time delay (as a function of the black hole spin) between the second and the first relativistic images appearing on the same side of a Kerr black hole.

get

$$\Delta\tilde{T}_{n,m}^o = \frac{\tilde{a}(a)}{\bar{a}(a)}[2\pi n + \gamma - \bar{b}(a)] + \tilde{b}(a) - \frac{\tilde{a}(-a)}{\bar{a}(-a)}[2\pi m - \gamma - \bar{b}(-a)] - \tilde{b}(-a) \quad (\text{A6})$$

and we see that now we also need the coefficients \bar{b} and \tilde{b} for the calculation, since they are not the same for the two images and do not cancel like in the spherically symmetric case.

Considering a source aligned behind the black hole ($\gamma = 0$), in Fig. 2 we plot the time delay between the second and first images appearing on the same side of the black hole. For positive a the two images are direct and for negative a they are both retrograde. We see that the time delay decreases if the images are both direct, while increases if they are both retrograde. We can also notice that the largest contribution to the time delay still comes from $\Delta\tilde{T}$, while the second term in (31) at most contributes for 6% when $a = 0.5$ and the last term stays below 0.7%.

The situation is quite different for images on opposite sides (Fig. 3). The time delay is zero when $a = 0$ and becomes negative for positive a . This means that direct light rays take less time than retrograde rays to wind around the black hole. This is naturally understood since the radius of the photon sphere is larger for retrograde light rays. For high values of the black hole spin, $\Delta T_{1,1}^o$ becomes comparable to $\Delta T_{2,1}^s$. Another interesting fact is that the second term in (31) is of the same order of the dominant term $\Delta\tilde{T}$, the ratio being roughly $-1/3$. The last term also contributes for 1.7%.

[1] F.W. Dyson, A.S. Eddington, C. Davidson, Phil. Trans. Roy. Soc. 220A, 291 (1920).

[2] P. Schneider, J. Ehlers, E.E. Falco, *Gravitational lenses*,

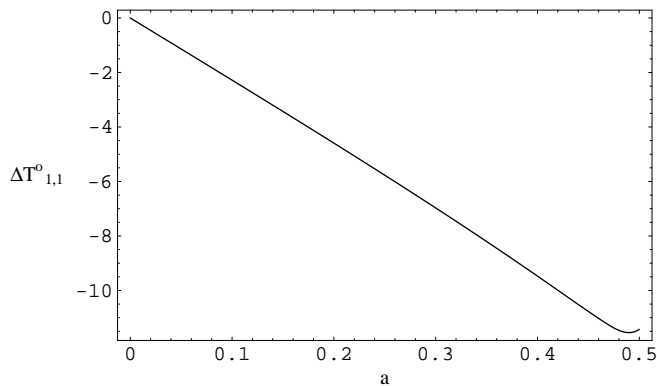


FIG. 3: Time delay (as a function of the black hole spin) between the first direct relativistic image and the first retrograde image.

Springer-Verlag, Berlin (1992).

- [3] R.D. Atkinson, *Astron. Jour.* **70**, 517 (1965).
- [4] K.S. Virbhadra, G.F.R. Ellis, *Phys. Rev. D* **62**, 084003 (2000).
- [5] S.U. Viergutz, *A&A* 272 (1993) 355.
- [6] R.J. Nemiroff, *Amer. Jour. Phys.* **61**, 619 (1993).
- [7] S. Frittelli, E.T. Newman, *Phys. Rev. D* **59**, 124001 (1999).
- [8] S. Frittelli, T.P. Kling, E.T. Newman, *Phys. Rev. D* **61**, 064021 (2000).
- [9] V. Perlick, gr-qc/0307072.
- [10] M.P. Dabrowski, F.E. Schunck, *Astroph. Jour.* **535**, 316 (2000).
- [11] H. Falcke, F. Melia, E. Agol, *ApJ Letters* 528 (1999) L13.
- [12] V. Bozza, S. Capozziello, G. Iovane, G. Scarpetta, *Gen. Rel. and Grav.* **33**, 1535 (2001).
- [13] E.F. Eiroa, G.E. Romero, D.F. Torres, *Phys. Rev. D* **66**, 024010 (2002).
- [14] A.O. Petters, *MNRAS* **338**, 457 (2003).
- [15] V. Bozza, *Phys. Rev. D* **66**, 103001 (2002).
- [16] A. Bhadra, *Phys. Rev. D* **67**, 103009 (2003).
- [17] V. Bozza, *Phys. Rev. D* **67**, 103006 (2003).
- [18] S.E. Vazquez, E.P. Esteban, gr-qc/0308023.
- [19] S. Refsdal, *MNRAS* **128**, 307 (1964).
- [20] R.D. Blandford, R. Narayan, *Ann. Rev. Astron. & Astroph.* **30**, 311 (1992).
- [21] D. Walsh, R.F. Carswell, R.J. Weymann, *Nature* **279**, 381 (1979).
- [22] ARISE web page: arise.jpl.nasa.gov; MAXIM web page: maxim.gsfc.nasa.gov; J.S. Ulvestad astro-ph/9901374.
- [23] D. Richstone et al., *Nature* **395**, A14 (1998).
- [24] P. Fouqué, J.M. Solanes, T. Sanchis, C. Balkowski, *Astron. and Astroph.* **375**, 770 (2001).